May 23

IN Press, 6/2000

Tropical convective outflow and near surface equivalent potential temperatures

Ian Folkins

Atmospheric Science Program, Dalhousie University, Halifax, Canada

Samuel J. Oltmans

NOAA Climate Monitoring and Diagnostics Laboratory, Boulder, CO

Anne M. Thompson

NASA/Goddard Space Flight Center, Greenbelt, Maryland

Geophysical Research Letters.

Short title: TROPICAL CONVECTIVE OUTFLOW AND NEAR SURFACE θ_E

Abstract. We use clear sky heating rates to show that convective outflow in the tropics decreases rapidly with height between the 350 K and 360 K potential temperature surfaces (or between roughly 13 and 15 km). There is also a rapid fall-off in the pseudoequivalent potential temperature probability distribution of near surface air parcels between 350 K and 360 K. This suggests that the vertical variation of convective outflow in the upper tropical troposphere is to a large degree determined by the distribution of sub cloud layer entropy.

Subcloud layer entropy plays an important role in determining the depth of convective mixing in the tropics [*Emanuel*, 1994]. Figure 1 shows two probability distributions of "near surface" pseudoequivalent potential temperature θ_e in the tropics. θ_e is a measure of entropy which includes the potential contribution arising from water vapor condensation. Its virtue in this context is that the θ_e of an air parcel is approximately conserved during upward transport within clouds provided there is no mixing. The cumulative probability distribution $N(\theta_e)$ shown in Figure 1 gives the fraction of air parcels below 1 km whose pseudoequivalent potential temperature is larger than a given θ_e. Approximately 7 % of the air parcels below 1 km in the tropics have a θ_e larger than 355 K. The curve $dN(\theta_e)/d\theta$ is the relative probability distribution of near surface θ_e obtained by counting the number of θ_e measurements in 1 K bins. It has been normalized so that its largest value is equal to 1. There is a rapid (roughly exponential) decrease in the occurrence of air parcels with θ_e larger than 355 K.

The distribution shown in Figure 1 is intended to represent an annual tropical average. It was compiled from temperature and humidity profiles from the following missions: the Pacific Exploratory Mission (PEM) - Tropics A and B, the Indian Ocean Experiment (INDOEX), and the Southern Hemisphere Additional Ozonesondes (SHADOZ) initiative. For simplicity, we will collectively refer to this dataset as the SHADOZ archive. It involved a total of 673 profiles - 93 from Ascension Island (8 °S). 4 from Christmas Island (2 °N), 77 from San Cristobal (1 °S), 114 from Fiji (18 °S), 23 from Watukosek Java (7.5 °S), 53 from Kaashidhoo (5 °N), 94 from Nairobi (1.3 °S), 40 from Natal (5.4 °S), and 175 from Samoa (14.2 °S). The average latitude, weighted by

the number of profiles, was 8.3 °S. There was an approximately equal number of sondes taken in each season. Since the sondes were taken at varying vertical resolution, a $N(\theta_e)$ was first calculated for each site, and then entered into the overall average in a weighted manner depending on the number of sondes at that site. Pseudoequivalent potential temperatures were calculated using the Bolton parameterization [*Bolton*, 1980].

The two main mechanisms which drive downward descent across isentropic surfaces in the tropics are radiative and evaporative cooling. The radiatively driven mass flux $M_r(\theta)$ can be approximated as

$$M_r(\theta) = \rho(\theta) w_r(\theta) = \rho(\theta) Q(\theta) / (dT(\theta)/dz + \Gamma_d). \tag{1}$$

Here $dT(\theta)/dz$ is the derivative of temperature with respect to height. Γ_d the dry adiabatic lapse rate, $\rho(\theta)$ density, $w_r(\theta)$ the downward radiative velocity, and $Q(\theta)$ the clear sky radiative cooling rate. This expression is valid in clear-sky regions over long timescales where the heights of potential temperature surfaces can be regarded as fixed.

The left hand side of Figure 2 shows the vertical variation of $M_r(\theta)$ in the upper tropical troposphere obtained from (1). The open circles represent the mass flux $M_r(\theta)$ while the solid circles represent $N(\theta_e)$, with in this case, the vertical axis understood to be θ_e rather than θ. The horizontal axes of $M_r(\theta)$ and $N(\theta_e)$ have been adjusted so that the two plots roughly coincide at $\theta = 348$ K. This has been done to emphasize that $M_r(\theta)$ and $N(\theta_e)$ are roughly proportional to one another for θ (or θ_e) larger than 345 K.

The simplest way to explain the scaling between $M_r(\theta)$ and $N(\theta_e)$ shown in Figure

2 is to assume (1) that near surface air parcels have a roughly equal probability of being subjected to deep convection, (2) that air parcels detrain from convective systems near their Level of Neutral Buoyancy (LNB), (3) that most of the downward descent in the tropics is driven by radiative cooling, and (4) that the radiative effect of clouds on the vertical mass flux is small. Although none of these assumptions can be expected to be correct in any exact sense, they may be sufficiently valid, at least above 345 K, to account for the scaling between $M_r(\theta)$ and $N(\theta_e)$ in this region.

The right hand side of Figure 2 shows that the vertical divergence of the radiatively driven mass flux, $dM_r(\theta)/dz$, roughly scales with the relative near surface θ_e probability distribution $dN(\theta_e)/d\theta_e$. This follows from the scaling between $M_r(\theta)$ and $N(\theta_e)$ and is shown for illustrative purposes. The divergence of $M_r(\theta)$ can be regarded as approximately equal to that part of the convective outflow which is driven by radiative cooling. $dM_r(\theta)/dz$ decreases somewhat less rapidly with height than does $dN(\theta_e)/d\theta_e$ for θ higher than 355 K. This would be consistent with a somewhat greater likelihood for deep convection in regions of higher near surface θ_e.

A three-dimensional modeling simulation gives the net mass flux at 10 km as approximately 0.004 $kgm^{-2}s^{-1}$, or 345 $kgm^{-2}day^{-1}$ [*Tompkins and Craig*, 1998]. Net mass flux in this case refers to the residual between the mass fluxes from convective updrafts and downdrafts, and should approximately equal M_r at 10 km, which from Figure 2 is about 350 $kgm^{-2}day^{-1}$. The manner in which modeled mass fluxes decrease with height above 10 km should be quite sensitive to their near surface θ_e distributions.

The clear-sky heating rates used in (1) were calculated using a radiative transfer

model based on the δ-four-stream method [*Fu and Liou,* 1992]. The annual tropical climatologies of temperature, water vapor, ozone, and pressure at 0.5 km resolution used in the model was obtained from the SHADOZ archive. Because of uncertainties in the accuracy of water vapor measurements above 12 km, we imposed a constant 3.8 ppmv water vapor mixing ratio above 17 km [*Dessler,* 1998], and used spline interpolation to determine the relative humidity between 12 and 17 km.

The climatological temperature and lapse rate profiles used in the radiative transfer model are plotted versus θ in Figure 3. It is interesting that the onset of scaling between $M_r(\theta)$ and $N(\theta)$, the peak of the near surface θ_e relative probability distribution, and the onset of an increase in lapse rate all occur between 345 and 350 K. By 370 K, the convective outflow (as diagnosed from the radiative mass flux) and the near surface θ_e relative probability distribution have essentially diminished to zero. This is below both the cold point (383 K) and lapse rate (375 K) definitions of the tropical tropopause, and is consistent with previous work based on GCM's [*Thuburn and Craig.* 1997], cloud top temperatures [*Highwood and Hoskins,* 1998], and ozone and lapse rate variations [*Folkins et al.,* 1999], that the traditional definitions of the tropical tropopause are not good indicators of the upper limit of convective mixing in the tropics.

Temperatures in the lower tropical stratosphere are lowest during Northern Hemisphere winter when the adiabatic cooling induced by upward ascent is strongest [*Yulaeva et al.,* 1994]. Tropospheric temperatures above Samoa (14 °S) are highest during Northern Hemisphere winter when the local solar insolation is strongest. In Figure 4, we have subtracted the average July-September (local winter) temperature

profile above Samoa from the average January-March (local summer) profile. The transition from tropospheric (positive temperature difference) to stratospheric (negative temperature difference) control occurs at 355 K, the approximate altitude at which the convective outflow shown in Figure 2 has diminished to half its maximum value.

Near surface $N(\theta_e)$ distributions at sites within the Western Pacific Warm Pool can be shifted by up to 5 K to the right of the tropical average shown in Figure 1. The scaling between $N(\theta_e)$ and $M_r(\theta)$ is a statistical relationship that can be expected to apply only over sufficiently long times and large distances. It would be interesting to see if the regional and seasonal variations of $N(\theta_e)$ and $M_r(\theta)$ coevolve in a manner consistent with the scaling shown here for tropical means.

There are several indications that water vapor concentrations in the stratosphere have increased over the past several decades [*Oltmans and Hofmann*, 1995]. This development may have important climate implications [*Forster and Shine*, 1999]. One explanation is that tropopause cold point temperatures have increased in response to surface warming [*Kirk-Davidoff et al.*, 1999]. Predicting the manner in which cold point temperatures will respond to global warming is made difficult by the fact that it is near a transition from radiative-convective (troposphere) to near radiative (stratosphere) equilibrium. Temperatures in the upper tropical troposphere may respond to surface warming in such a way as to maintain the scaling between upper tropospheric mass fluxes and the near surface θ_e distributions shown in Figure 2. If so, these constraints may give some insight into how temperatures in this important transition region can be expected to evolve.

Acknowledgments. Sonde data for Samoa and Fiji were provided through the GTE database, archived at http://www-gte.larc.nasa.gov/, while all other sondes were provided through the SHADOZ database archived by J. C. Witte (SMAC at NASA-Goddard): http://code916.gsfc.nasa.gov/Data_services/shadoz. I. F. was supported by the Natural Sciences and Engineering Research Council of Canada.

References

Bolton, D., The computation of equivalent potential temperature, *Mon. Wea. Rev., 108*, 1046-1053, 1980.

Dessler, A. E., A reexamination of the "stratospheric fountain" hypothesis, *Geophys. Res. Lett., 25*, 4165-4168, 1998.

Emanuel, K. A., Atmospheric Convection, Oxford University Press, 1994.

Folkins, I., M. Loewenstein, J. Podolske, S. Oltmans, and M. Proffitt, A barrier to vertical mixing at 14 km in the tropics: Evidence from ozonesondes and aircraft measurements, *J. Geophys. Res., 104*, 22095-22101, 1999.

Forster, P. M., and K. P. Shine, Stratospheric water vapor changes as a possible contributor to observed stratospheric cooling, *Geophys. Res. Lett., 26*, 3309-3312, 1999.

Fu, Q., and K. N. Liou, On the correlated k-distribution method for radiative transfer in nonhomogeneous atmospheres, *J. Atmos. Sci., 49*, 2139-2156, 1992.

Highwood, E. J., and B. J. Hoskins, The tropical tropopause, *Q. J. R. Meteorol. Soc., 124*, 1579-1604, 1998.

Kirk-Davidoff, D. B., E. J. Hinsta, J. G. Anderson, and D. W. Keith, The effect of climate change on ozone depletion through changes in stratospheric water vapor, *Nature*, 402, 399-401, 1999.

Oltmans, S. J., and D. J. Hofmann, Increase in lower-stratospheric water vapour at a mid-latitude Northern Hemisphere site from 1981 to 1994, *Nature, 374*, 146 - 149, 1995.

Thuburn, J., and G. C. Craig, GCM tests of theories for the height of the tropopause, *J. Atmos. Sci.*, 54, 869-882, 1997.

Tompkins, A. M., and G. C. Craig, Radiative-convective equilibrium in a three dimensional cloud-ensemble model, *Q. J. R. Meteorol. Soc.*, **124**, 2073-2097, 1998.

Yulaeva, E., J. R. Holton, and J. M. Wallace, On the cause of the annual cycle in the tropical lower stratospheric temperature, *J. Atmos. Sci., 51*, 169-174, 1994.

I. Folkins. Department of Oceanography, Dalhousie University, Halifax, Nova Scotia, Canada, B3H 4J1. (email: Ian.Folkins@dal.ca)

S. Oltmans, NOAA CMDL, 325 Broadway, Boulder, CO, USA, 80303. (email: soltmans@cmdl.noaa.gov)

A. Thompson, NASA/GSFC, Code 916, Greenbelt, Md, USA 20771. (email: thompson@gator1.gsfc.nasa.gov)

Received XXXX XX, 2000; revised XXXX XX, 2000; accepted XXXX XX, 2000.

Figure 1. Two probability distributions of near surface (below 1 km) θ_e values in the tropics. $N(\theta_e)$ is the cumulative probability distribution representing the fraction of air parcels whose θ_e is larger than a given value. $dN(\theta_e)/d\theta$ is the relative probability distribution obtained by counting the number of θ_e measurements within a given θ_e interval, in this case 1 K. The peak of this distribution has been arbitrarily normalized to 1. Both distributions were obtained from the SHADOZ archive.

Figure 2. (left) The curve with open circles is the clear sky vertical mass flux $M_r(\theta)$ as obtained from (1) in the text. The curve with solid circles is $N(\theta_e)$ from Figure 1, but with the axes interchanged. (right) The curve with open circles is $dM_r(\theta)/dz$. The curve with solid circles is $dN(\theta_e)/d\theta$, also from Figure 1 with the axes interchanged.

Figure 3. Temperature and lapse rate (here dT/dz rather than -dT/dz) versus potential temperature, from the SHADOZ archive. The lapse rate tropopause is usually defined as the altitude at which temperature decreases less rapidly than 2 K/km.

Figure 4. Local Summer (January through March) minus local winter (July through September) temperatures above Samoa.

Figure 1

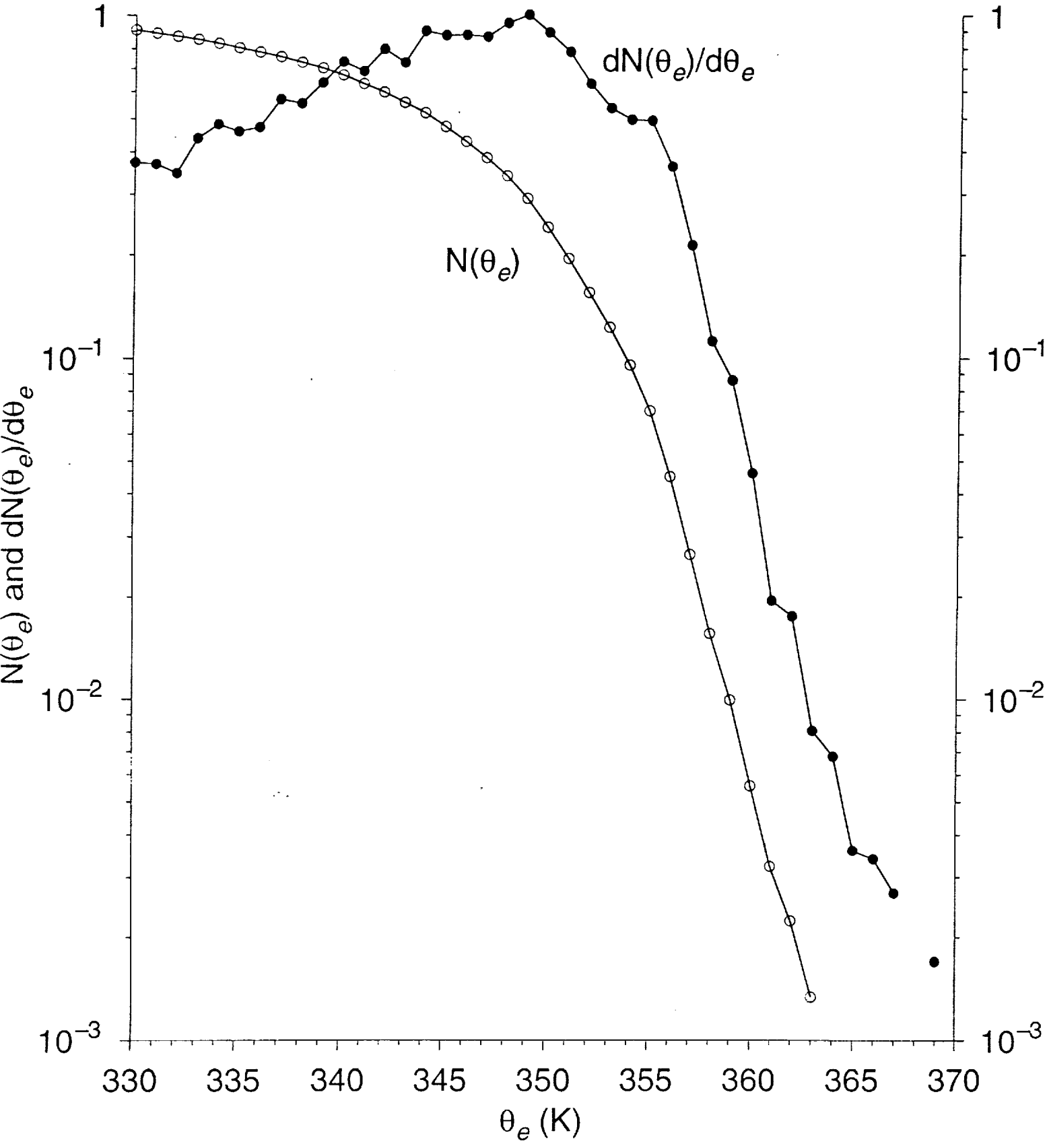
1
10^{-1}
10^{-2}
10^{-3}
$dN(\theta_e)/d\theta_e$
$N(\theta_e)$
$N(\theta_e)$ and $dN(\theta_e)/d\theta_e$
330
335
340
345
350
355
360
365
370
θ_e (K)

Figure 2

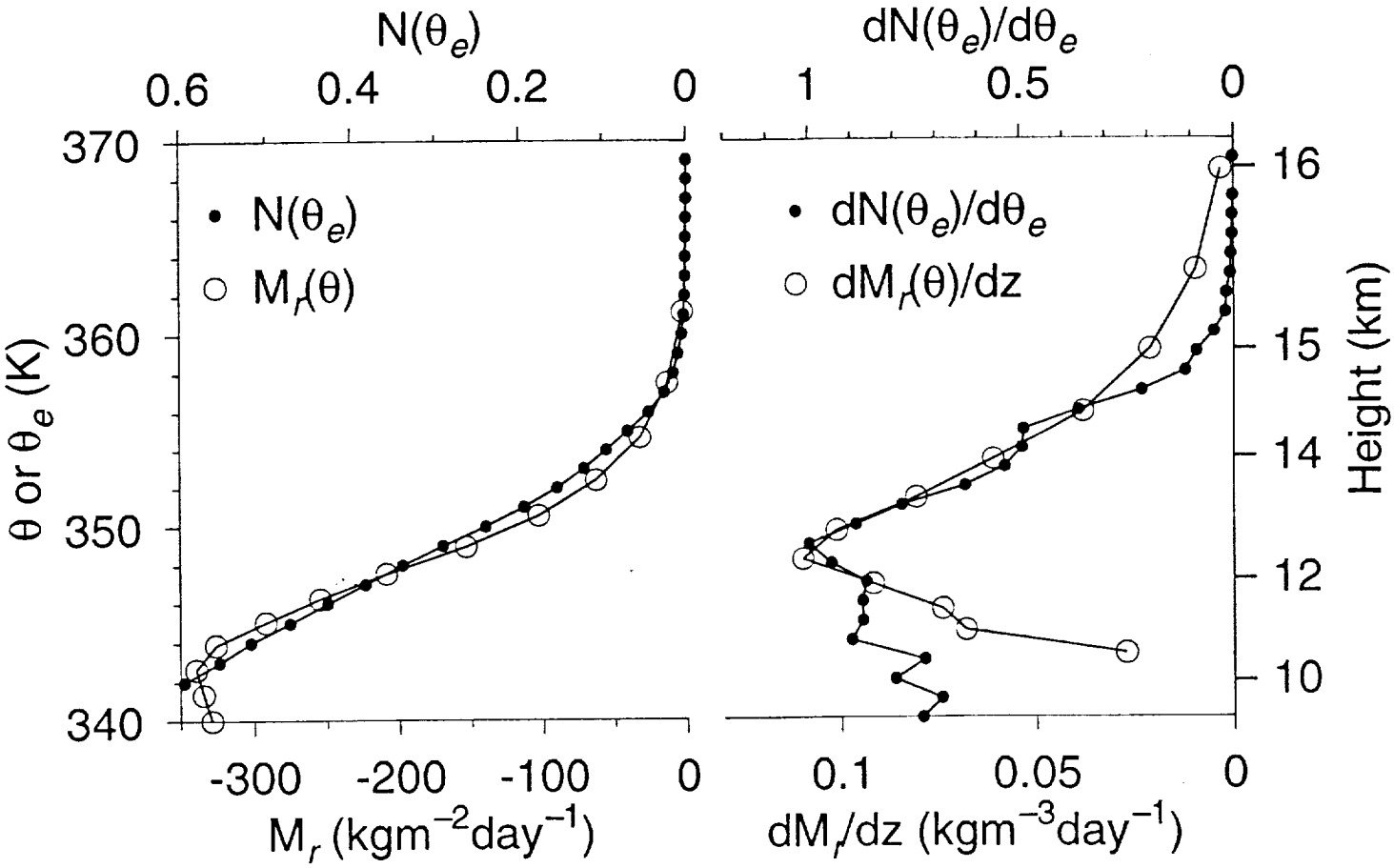
N(θe)
0.6
0.4
0.2
0
dN(θe)/dθe
1
0.5
0
370
360
350
340
θ or θe (K)
• N(θe)
○ Mr(θ)
• dN(θe)/dθe
○ dMr(θ)/dz
16
15
14
12
10
Height (km)
-300
-200
-100
0
Mr (kgm−2day−1)
0.1
0.05
0
dMr/dz (kgm−3day−1)

Figure 3

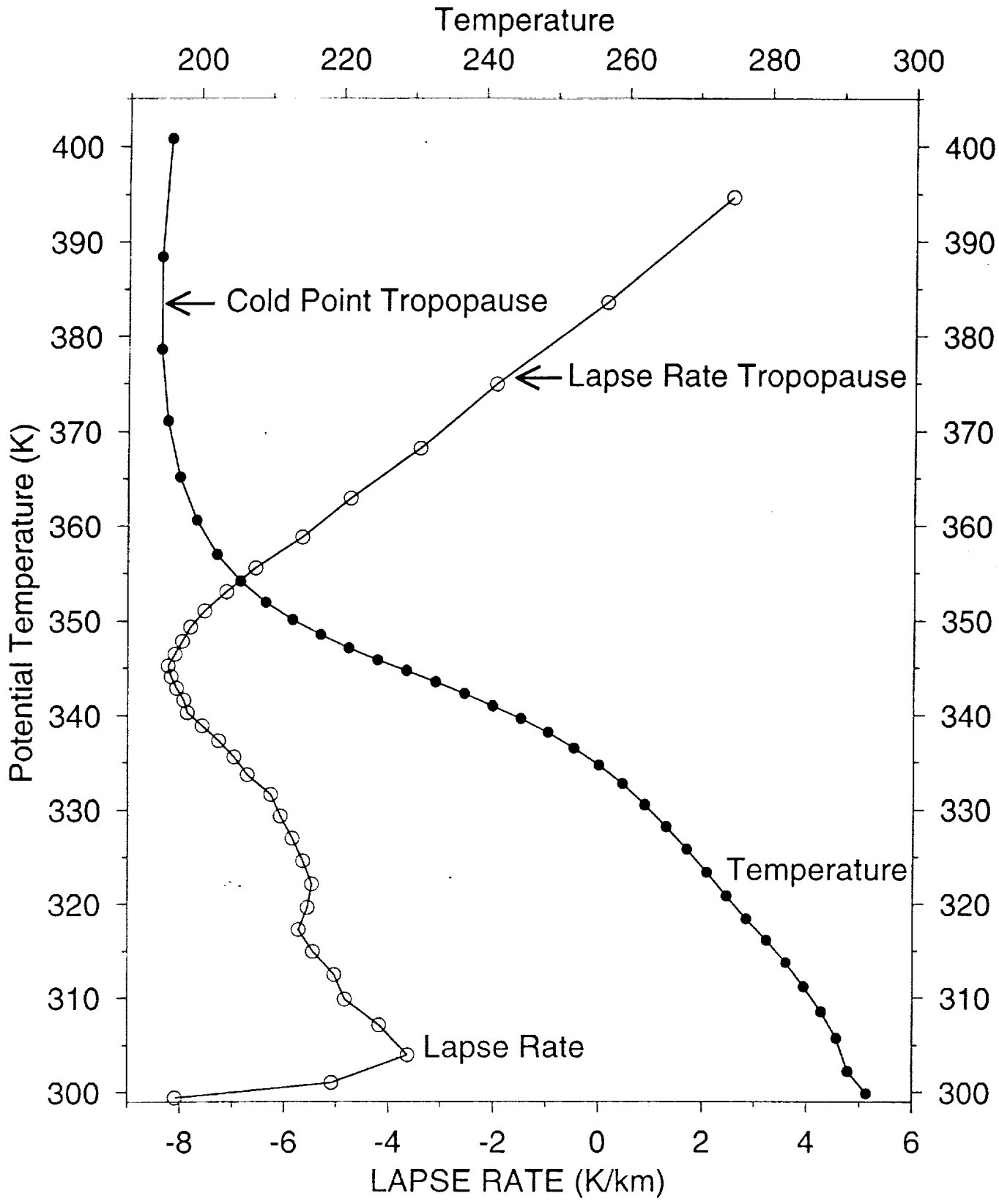
Temperature
200
220
240
260
280
300
400
390
380
370
360
350
340
330
320
310
300
Potential Temperature (K)
Cold Point Tropopause
Lapse Rate Tropopause
Temperature
Lapse Rate
-8
-6
-4
-2
0
2
4
6
LAPSE RATE (K/km)

Figure 4

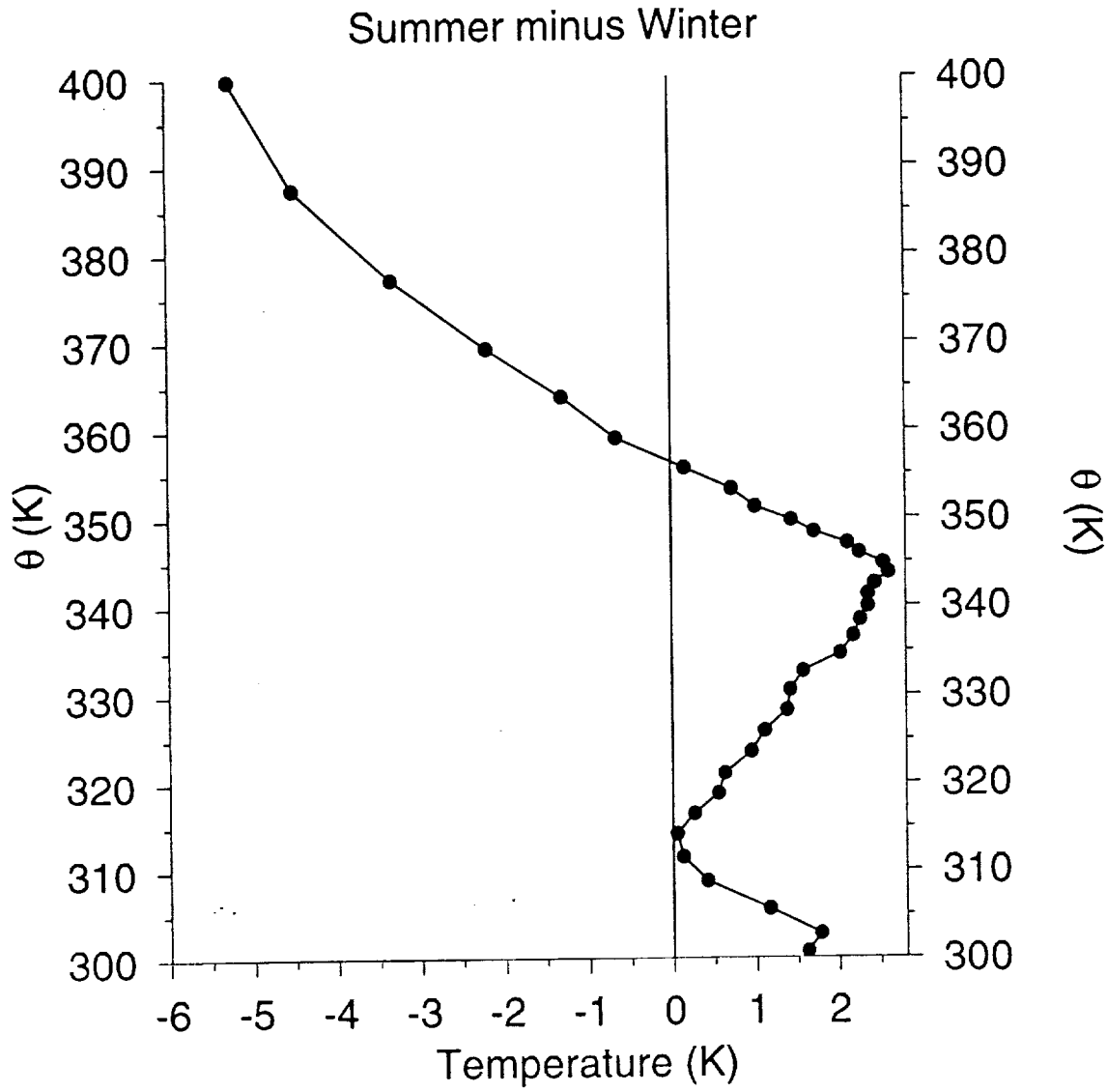
Summer minus Winter
400
390
380
370
360
350
340
330
320
310
300
θ (K)
-6
-5
-4
-3
-2
-1
0
1
2
Temperature (K)